CO_2 abatement by two-dimensional MXene carbides

Ángel Morales-García, Adrián Fernández-Fernández, Francesc Viñes* and Francesc Illas

Departament de Ciència de Materials i Química Fisica & Institut de Química Teòrica i Computacional (IQTCUB), Universitat de Barcelona, c/Martí i Franquès 1, 08028 Barcelona, Spain.

**E-mail:* francesc.vines@ub.edu

1. Computational Aspects: Methods and Models

All calculations have been carried out using the density functional theory (DFT)[1,2] formalism with the generalized gradient approximation (GGA) of Perdew, Burke, and Ernzerhof (PBE),[3] as implemented in the Vienna *ab initio* simulation (VASP) package.[4,5] The D3 dispersion correction proposed by Grimme[6] was also applied on PBE (PBE-D3). Projector augmented wave (PAW) potentials[7] were used to describe the electron-ionic core interaction. Brillouin zone integration was sampled using the Monkhorst and Pack method[8] by 5×5×1 **k**-grid mesh. The valence electron density was expanded in a plane wave basis set with a cut-off energy of 415 eV. The threshold for the electronic optimization was set to 10^{-5} eV, and geometry optimizations were considered converged when forces acting on atoms were below 0.01 eV/Å.

Transition metal carbides MXene models were built from the removal of A group layer from the MAX phase, where M represents a transition metal (M = Ti, V, Cr, Zr, Nb, Mo, Hf, Ta and W), X denotes C, and A is an A-group (mostly IIIA and IVA, or groups 13 and 14) elements.[9,10] The modeled MXenes contain three atomic layers forming a M-C-M sandwich, *i.e.* M_2C structure (see Figure S1) with the (0001) orientation exposed. A (3×3) supercell containing 18 M and 9 C atoms, was used and prior optimized to study the adsorption of CO_2. All atomic layers and CO_2 were allowed to relax during the CO_2 adsorption processes. A vacuum of 10 Å was inserted to avoid the interaction between the slabs. The CO_2 molecule with an PBE C-O distance of 1.176 Å was placed in several sites with different orientations respect on MXene (0001) direction (see Figure S1). Here, the adsorption energy, E_{ads}, is defined as,

$$E_{ads} = E_{CO_2/MXene} - \left(E_{MXene} + E_{CO_2}\right) + E_{ZPE} \quad (1)$$

where $E_{CO_2/MXene}$ is the energy of CO_2 adsorbed on the corresponding MXene surface. E_{MXene} and E_{CO_2} stand for the energy of the relaxed pristine MXene surface and the energy of an isolated CO_2 molecule,

respectively. E_{CO_2} was calculated at the **Γ**-point in a symmetric box of 10×10×10 Å dimensions, and E_{ZPE} corresponds to zero-point energy (ZPE) of CO_2 molecule in the harmonic approximation. Note that ZPE is considered for both gas phase and adsorbed CO_2. Attending to Eq. (1), the stronger adsorption is associated with the more negative E_{ads}. Note that the vibrational frequencies were calculated decoupled from surface phonons and including frustrated rotations/translations.

To distinguish the CO_2 adsorption sites on the MXene surface, we use a coordination notation pointing out firstly a digit (n) related with the number of CO_2 atoms (3, 2, or 1) linked on the surface (η^n-CO_2) depending on the orientation of the adsorbed CO_2 molecule (see side view in Figure S1), followed then by a second digit (m) associated to the atomic environment (5, 3, or 2) occupied by the CO_2 molecule (μ^m), finally followed by a specification of the location of the n-contacting molecule atoms (C, M, or B which correspond to Carbon hollow, Metal hollow, or Bridge positions). For instance, Figure S1a shows a flat orientation of the CO_2 with three atoms connected to the surface (η^3-CO_2) with an atomic environment of 5 surface Metal atoms (μ^5). Finally, the CO_2 carbon atom is located on C top site of the middle layer (C_C) and both oxygens on M top of the bottom layer (O_M). Looking at the side sketches in Figure S1, we identify five different sites depending on the features described above.

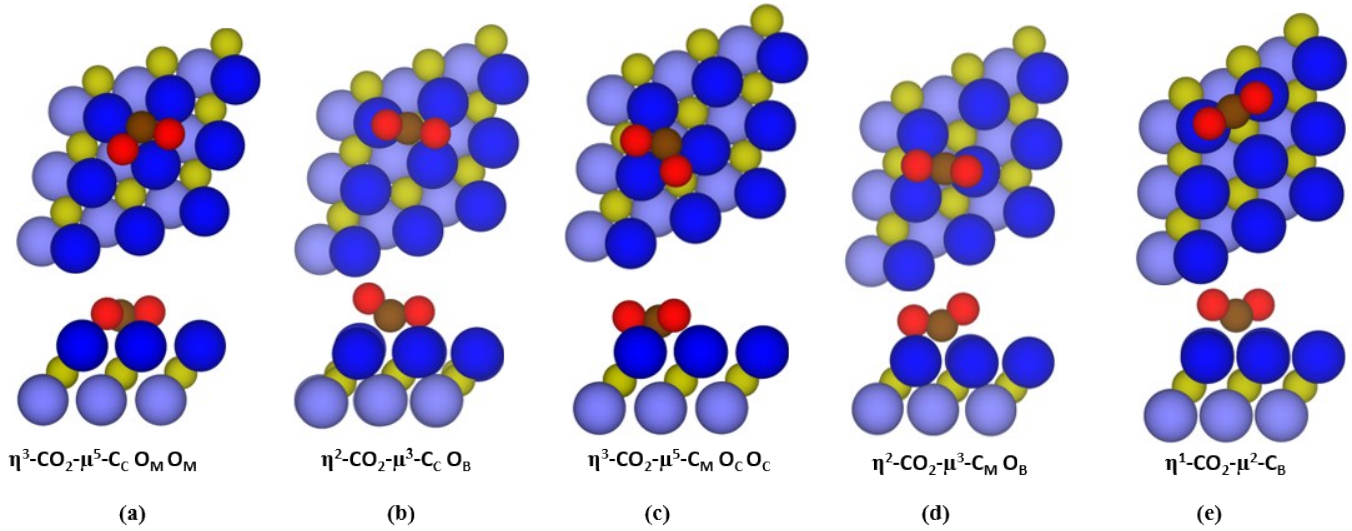

Figure S1. Top and side sketches of CO_2 adsorbed on (a) η^3-CO_2-μ^5-$C_CO_MO_M$, (b) η^2-CO_2-μ^3-C_CO_B, (c) η^3-CO_2-μ^5-$C_MO_CO_C$, (d) η^2-CO_2-μ^3-C_MO_B, (e) η^1-CO_2-μ^2-C_B sites. The CO_2 molecule is depicted with brown and red spheres which correspond to oxygen and carbon atoms, respectively. Layered MXene is described by two dark (top M layer) and light (bottom M layer) blue colors to distinguish the metals of different layers and dark yellow spheres correspond to the carbon middle layer of the MXene material, so to differentiate to the carbon of the CO_2 molecule.

2. Interaction of CO_2 with MXenes

Table S1 compiles the adsorption energies of CO_2 on MXene surfaces along with the C-O and M-O bond lengths, δ(CO) and δ(MO), respectively, the CO_2 molecular angle α(OCO), and the Bader charge difference (ΔQ) between the adsorbed and isolated CO_2 molecule. The information is presented itemized per site as shown in Figure S1. Note that calculations show a surface-bound anionic $CO_2^{\delta-}$ species with bent geometry (see α(OCO) and ΔQ indicators in Table S1). Several studies have evidenced the key role of this activation in further reaction of CO_2.[11] Previous studies have shown that experimental findings are compatible with the formation of the metastable $CO_2^{\delta-}$ with a bent geometry.[12] The bent anionic structure has larger C-O distances, 1.31-1.47 Å, than the isolated and neutral molecule, 1.16 Å. Our structural analysis reported in Table S1 indicates the formation of $CO_2^{\delta-}$ once the molecule is adsorbed, being consistent with the previous studies.[12]

Table S1. Adsorption energy (in eV) of CO_2 molecule on MXene carbides at PBE and PBE-D3 levels on the adsorption sites described in Figure S1. Bond lengths δ(CO) and δ(MO) are given in Å, as well as the CO_2 molecular angle, α(OCO), in degrees. The Bader charge analysis, ΔQ, are given in *e* and corresponds to charge difference between the adsorbed and isolated CO_2 molecule.

MXene	Level	E_{ads}[a]	δ(MO)	δ(CO)	α(OCO)	ΔQ
		η^3-CO_2-μ^5-$C_CO_MO_M$				
Ti_2C	PBE	-3.36	2.15 ; 2.21	1.38 (×2)	115.1	-1.85
	PBE-D3	-3.69	2.15 ; 2.21	1.39 (×2)	115.1	-1.85
V_2C	PBE	-1.71	2.07 ; 2.31 2.20 ; 2.21	1.47 1.33	113.5	-1.68
	PBE-D3	-2.41	2.08 ; 2.30 2.19 ; 2.20	1.47 1.33	113.6	-1.69
Zr_2C	PBE	-3.05	2.05 (×2)	1.34 (×2)	115.3	-1.32
	PBE-D3	-3.16	2.05 (×2)	1.34 (×2)	115.3	-1.32
Nb_2C	PBE	-1.62	2.37 ; 2.44 2.21 ; 2.26	1.31 1.48	113.4	-1.63
	PBE-D3	-2.03	2.37 ; 2.44 2.21 ; 2.25	1.31 1.50	113.2	-1.64
Hf_2C	PBE	-3.08	2.27 ; 2.31 2.26 ; 2.31	1.37 1.39	115.0	-2.50
	PBE-D3	-3.36	2.27 ; 2.31 2.25 ; 2.31	1.37 1.40	115.0	-2.51
W_2C	PBE	-0.83	2.05 (×2)	1.34 (×2)	115.3	-1.33
	PBE-D3	-1.31	2.05 (×2)	1.34 (×2)	115.3	-1.33
		η^3-CO_2-μ^5-$C_MO_CO_C$				
Ti_2C	PBE	-3.15	2.18 ; 2.23	1.38 (×2)	115.8	-1.87
	PBE-D3	-3.47	2.17 ; 2.23	1.39 (×2)	115.7	-1.89
V_2C	PBE	-1.67	2.23 ; 2.27 2.08 ; 2.10	1.47 1.31	114.1	-1.64
	PBE-D3	-2.36	2.23 ; 2.26 2.08 ; 2.10	1.48 1.31	114.0	-1.63
Zr_2C	PBE	-2.92	2.35 ; 2.36 2.36 ; 2.37	1.37 1.36	116.3	-1.78
	PBE-D3	-3.03	2.35 ; 2.36	1.37 1.36	116.3	-1.78
Nb_2C	PBE	-1.61	2.33 ; 2.39	1.35	117.5	-1.59

			2.32 ; 2.42	1.34		
	PBE-D3	-2.01	2.33 ; 2.39	1.35	117.5	-1.59
			2.32 ; 2.42	1.34		
Hf_2C	PBE	-3.05	2.30 ; 2.31	1.39	115.2	-2.85
			2.31 ; 2.32	1.37		
	PBE-D3	-3.33	2.29 ; 2.31	1.39	115.2	-2.86
			2.31 (×2)	1.37		
Ta_2C	PBE	-1.97	1.36 (×2)	1.36 (×2)	113.8	-1.69
			2.02 (×2)			
	PBE-D3	-2.37	1.36 (×2)	1.36 (×2)	113.8	-1.69
			2.02 (×2)			
			η^1-CO_2-μ^2-C_B			
V_2C	PBE	-1.38	2.11 (×2)	1.28 (×2)	132.7	-1.16
	PBE-D3	-2.05	2.10 (×2)	1.28 (×2)	132.7	-1.16
Nb_2C	PBE	-1.60	2.25 (×2)	1.28 (×2)	131.2	-1.19
	PBE-D3	-1.99	2.25 (×2)	1.28 (×2)	131.1	-1.19
Mo_2C	PBE	-1.32	2.23 (×2)	1.26 (×2)	134.3	-0.88
	PBE-D3	-1.61	2.23 (×2)	1.26 (×2)	134.4	-0.89
Ta_2C	PBE	-1.48	2.21 (×2)	1.28 (×2)	131.9	-1.23
	PBE-D3	-1.87	2.21 (×2)	1.28 (×2)	131.9	-1.23
W_2C	PBE	-0.66	2.24 (×2)	1.26 (×2)	135.1	-0.90
	PBE-D3	-1.13	2.24 (×2)	1.26 (×2)	135.1	-0.90
			η^2-CO_2-μ^3-C_MO_B			
V_2C	PBE	-1.62	2.11 ; 2.23	1.42	125.7	-1.53
			2.23	1.27		
	PBE-D3	-2.32	2.10 ; 2.22	1.44	125.1	-1.57
			2.24	1.27		
Nb_2C	PBE	-1.75	2.38 (×2)	1.33	130.2	-1.41
			2.37	1.27		
	PBE-D3	-2.11	2.37 (×2)	1.33	130.3	-1.42
			2.36	1.27		
Mo_2C	PBE	-1.33	2.34 (×2)	1.32	132.7	-1.16
			2.39	1.26		
	PBE-D3	-1.63	2.33 (x2)	1.32	132.8	-1.16
			2.38	1.26		
Ta_2C	PBE	-1.51	2.34 ; 2.35	1.34	130.6	-1.51
			2.36	1.27		
	PBE-D3*	-2.37	1.36 (×2)	1.36 (×2)	113.8	-1.68
			2.02 (×2)			
			η^2-CO_2-μ^3-C_CO_B			
Ti_2C	PBE	-2.57	2.25	1.28	131.6	-1.68
			2.20 (×2)	1.38		
	PBE+D3	-2.88	2.25	1.28	131.7	-1.71
			2.20 (×2)	1.38		
Mo_2C	PBE	-1.17	2.35	1.26	133.2	-1.10
			2.34(×2)	1.31		
	PBE+D3	-1.47	2.34	1.26	133.4	-1.12
			2.33 (×2)	1.31		

[a] ZPE corrected as stated above.

***** After optimization at PBE-D3 level, the CO_2 molecule is found to be stable in η^3-CO_2-μ^5-$C_MO_CO_C$ instead of η^2-CO_2-μ^3-C_MO_B as it found at PBE level.

3. Model of adsorption/desorption rates

The equation for an elementary reaction rate r_i is obtained from the Transition State Theory (TST)[13] by

$$r_i = v \cdot exp\left(-\frac{\Delta E}{k_B \cdot T}\right); v = \frac{k_B \cdot T_q^{\#}}{h \cdot q_0} \qquad (2)$$

where k_BT is the product of Boltzmann constant, k_B, and the temperature, T, and ΔE would be associated to the energy barrier for the described transition. In Eq. (2), v is a pre-factor term obtained from TST with h, $q^{\#}$ and q_0 being the Planck constant, partition functions of the transitions and initial states, respectively.

The rate of adsorption, r_{ads}, depends on the influence of adsorbates on the surface. For a non-activated adsorption, it can be calculated r_{ads} from Eq. (2) by adding the ratio of partition functions for a molecule in gas phase and in an early 2D transition state,[14,15]

$$r_{ads} = \frac{S_0 \cdot p_{CO_2} \cdot A}{\sqrt{2\pi \cdot m \cdot k_B \cdot T}} \quad (3)$$

where S_0 is the initial sticking coefficient, p_{CO_2} is the CO_2 partial pressure above the surface, A stands for the area of an adsorption site and m corresponds to the mass of the CO_2 molecule. A conservative value S_0 = 0.40 was selected for our study following a previous analysis where the CO_2 capture, storage and activation were investigated on transition metal carbides (TMC).[14] Equal adsorption probabilities of all sites (Figure S1) were assumed and therefore, A was calculated by dividing the supercell area of each surface by the total number of sites in it.[14] Adsorption rates have been calculated for *i*) the current atmospheric partial pressure of CO_2, p_{CO_2} = 40 Pa,[16] *ii*) for a partial pressure of p_{CO_2}= 0.15 bar ($1.5 \cdot 10^3$ Pa), a benchmark value for post-combustion exhaust gases,[17] and *iii*) p_{CO_2}= 1.0 bar (10^5 Pa), a partial pressure regime of interest for pure CO_2 stream generation from a carbon capture and storage (CCS) system.[18]

The rate of desorption, r_{des}, has been also obtained from eq. (2) using the E_{ads} values. Note that E_{ads} is negative by definition and ZPE corrected,

$$r_{des} = v_{des} \cdot exp\left(\frac{E_{ads}}{k_B \cdot T}\right); v_{des} = \frac{k_B \cdot T \cdot q^{gas}_{trans,2D} \cdot q^{gas}_{rot} \cdot q^{gas}_{vib}}{q^{ads}_{vib}} \quad (4)$$

where the pre-factor for v_{des} contains the partition function of the molecule in an early 2D transition state in the numerator. This partition function is given by the product $q^{gas}_{trans,2D} \cdot q^{gas}_{rot} \cdot q^{gas}_{vib}$ in which $q^{gas}_{trans,2D}$ stands for the partition function for translational motion in two dimensions whereas, q^{gas}_{rot} and q^{gas}_{vib} the rotational and vibrational partition functions in the gas phase. Once the molecule is adsorbed on the surface all degrees of freedom are considered as vibrations since molecular translations and rotations become frustrated by the substrate, and so, effectively converted into vibrations. The partition function

q_{vib}^{gas} only contains vibrational contributions. It must be noted that the electronic partition function was set to 1 given the excited electronic states lie high in energy. The partition functions were evaluated as

$$q_{trans,\,2D}^{\;gas} = A \cdot \frac{2\pi \cdot k_B \cdot T}{h^2} \tag{5}$$

$$q_{vib}^{ads/gas} = \prod_i \frac{exp\left(-\frac{h \cdot v_i}{2 \cdot k_B \cdot T}\right)}{1 - exp\left(-\frac{h \cdot v_i}{k_B \cdot T}\right)} \tag{6}$$

$$q_{rot}^{gas} = \frac{T}{2 \cdot T_{rot}} \tag{7}$$

where v_i is the vibrational frequency of each normal mode as obtained from our DFT calculations, either for CO_2 molecule in vacuum or adsorbed. $2 \cdot T_{rot}$ is the product of the rotational temperature for CO_2 and its symmetry number, 2. T_{rot} is taken as 0.561 K from the literature.[19]

This adsorption/desorption rate model allows one to calculate the rates for desorption and adsorption of CO_2 on MXene (0001) surfaces. Table S2 shows the desorption temperature range for each one of the adsorption sites studied (see Figure S1). The reported temperature range is interpreted as the range in which MXene surface loses its capacity to initially capture and accumulate CO_2 when annealing.

Table S2. Desorption temperature range ([PBE]–[PBE-D3]) for CO_2 partial pressure ranges for CO_2 partial pressures of 40, $15 \cdot 10^3$, and 10^5 Pa, which stand for air, exhaust and desorption, respectively. All temperature values are in K.

MXene	**Temp. range**		
	air	**exhaust**	**desorption**
η^3-CO_2-μ^5-$C_CO_MO_M$			
Ti_2C	1456-1598	1897-2084	2101-2312
V_2C	731-1034	938-1340	1034-1477
Zr_2C	1302-1351	1690-1754	1869-1938
Nb_2C	715-888	928-1154	1024-1280
Hf_2C	1309-1432	1695-1855	1874-2054
W_2C	344-535	426-665	461-731
η^3-CO_2-μ^5-$C_MO_CO_C$			
Ti_2C	1365-1511	1779-1976	1974-2194
V_2C	713-1017	918-1317	1009-1456
Zr_2C	1235-1281	1598-1659	1765-1831
Nb_2C	699-856	900-1103	997-1218
Hf_2C	1279-1397	1648-1804	1819-1991
Ta_2C	799-948	1014-1202	1112-1315

η^1-CO_2-μ^2-C_B			
V_2C	601-903	782-1178	866-1310
Nb_2C	712-874	930-1141	1037-1267
Mo_2C	561-677	721-869	793-957
Ta_2C	630-787	812-1013	896-1116
W_2C	470-696	600-896	657-992
η^2-CO_2-μ^3-C_MO_B			
V_2C	729-1046	949-1383	1052-1547
Nb_2C	781-888	1023-1155	1135-1279
Mo_2C	576-696	740-898	819-990
Ta_2C	688-946	904-1200	1007-1315
η^2-CO_2-μ^3-C_CO_B			
Ti_2C	1085-1210	1384-1543	1517-1694
Mo_2C	499-618	640-790	705-870

4. Quantitative adsorption of CO_2 by MXenes

The effectiveness of MXene materials is also investigated to quantify the amount of CO_2 adsorbed per MXene amount as mol CO_2/kg. of substrate (or mmol CO_2/g. of substrate). For this purpose we assumed that four CO_2 molecules could be simultaneously adsorbed on each one of the MXene layers within the employed (3×3) supercell, giving a total of 8 CO_2 molecules (upper and bottom layers covered by CO_2). Table S3 encompasses the estimated CO_2 uptake for MXene surfaces along with experimental evidences of zeolites, metal-organic-frameworks (MOFs), active carbons, and graphene and derivates.[20]

Table S3. Comparison of CO_2 adsorption capacity of MXene with other solid adsorbents: zeolites, MOFs, MgO nanopowders,[21] graphene & derivatives (further details in Ref. 20 and references therein).

Material	**CO_2 uptake**	
	g. CO_2/g. substrate	mol CO_2/kg. substrate
MXene		
Ti_2C	0.36	8.25
V_2C	0.34	7.80
Zr_2C	0.20	4.57
Nb_2C	0.20	4.49
Mo_2C	0.19	4.36
Hf_2C	0.11	2.41
Ta_2C	0.10	2.37
W_2C	0.10	2.34
Zeolites		

Ca-X	—	3.36
I3X	—	3.96
MOFs		
Cu-BTTri-mmen	—	2.38
MgO nanopowders	—	0.92
Graphene & derivatives		
a-RGO-750	—	2.18
a-RGO-850	—	2.75
a-RGO-950	—	3.36

REFERENCES

(1) P. Hohenberg and W. Kohn, *Phys. Rev.*, 1964, **136**, B864.

(2) W. Kohn and L. J. Sham, *Phys. Rev.*, 1965, **140**, A1133.

(3) J. P. Perdew, K. Burke and M. Ernzerhof, *Phys. Rev. Lett.*, 1996, **77**, 3865.

(4) G. Kresse and J. Furthmuller, *Comput. Mater. Sci.*, 1996, **6**, 15-50.

(5) G. Kresse and J. Furthmuller, *Phys. Rev. B*, 1996, **54**, 11169.

(6) S. Grimme, J. Anthony, S. Ehrlich and H. Krieg, *J. Chem. Phys.*, 2010, **132**, 154104.

(7) P. E. Blochl, *Phys. Rev. B*, 1994, **50**, 17953.

(8) H. J. Monkhorst and J. D. Pack, *Phys. Rev. B*, 1976, **13**, 5188.

(9) M. Naguib, V. N. Mochalin, M. W. Barsoum and Y. Gogotsi, *Adv. Mater.*, 2014, **26**, 992.

(10) M. Naguib and Y. Gogotsi, *Acc. Chem. Res.*, 2015, **48**, 128.

(11) H. J. Freud and M. W. Roberts, *Surf. Sci. Rep.*, 1996, **25**, 225.

(12) D. Schröder, C. A. Schalley, J. N. Harvey and H. Schwarz, *Int. J. Mass Spectrom.*, 1999, **185**, 25.

(13) K. Reuter, in *Modeling and Simulation of Heterogeneous Catalytic Reactions*, Wiley-VCH Verlag GmbH & Co. KGaA, 2011, ch. 3.

(14) S. Pogodin and N. López, *ACS Catal.*, 2014, **4**, 2328.

(15) C. Kunkel, F. Viñes and F. Illas, *Energy Environ. Sci.*, 2016, **9**, 141.

(16) T. Takahashi, S. Sutherland and A. Kozyr, *Global Ocean Surface Water Partial Pressure of CO_2 Database: Measurements Performed During 1957–2014 (Version 2014)*. Environmental Sciences Division, Oak Ridge National Laboratory, 2015.

(17) D. M. D'Alessandro, B. Smit and J. R. Long, *Angew. Chem. Int. Ed.*, 2010, **49**, 6058.

(18) M. E. Boot-Handford, J. C. Abanades, E. J. Anthony *et al.*, *Energy Environ. Sci.*, 2014, **7**, 130.

(19) P. W. Atkins and J. de Paula, *Atkins´ Physical Chemistry*, Oxford University Press, 8th edn., 2006.

(20) S. Chowdhury and R. Balasubramanian, *Ind. Eng. Chem. Res.*, 2016, **55**, 7906-7916.

(21) W. Gao, T. Zhou, B. Louis, Q. Wang, *Catalysts* 2017, **7**, 116.